Preprints of the 21st IFAC World Congress (Virtual)
Berlin, Germany, July 12-17, 2020

An Observer for the Electrically Heated Vertical Rijke Tube with Nonlinear Heat Release

Nils Christian A. Wilhelmsen * **Florent Di Meglio** *

* *Centre Automatique et Systèmes, MINES ParisTech, PSL Research University, 75006 Paris, France (e-mail: nils.wilhelmsen@mines-paristech.fr, florent.di_meglio@mines-paristech.fr)*

Abstract: This paper proposes an observer for the electrically heated vertical Rijke tube, using a model capable of inciting thermoacoustic instabilities. The model consists of linear, distributed acoustics coupled with nonlinear, lumped heat release. Using a boundary pressure measurement taken at the bottom end of the tube, the observer is designed by copying the system model and reconstructing both the bottom and top boundary conditions, the former exactly and the latter with an error that is shown to be converge to zero exponentially. It is proven that the observer produces state estimates that converge to their correct values asymptotically. Furthermore, it is shown the state estimation errors stay bounded when there is a modelling error in the boundary acoustic impedance. The proposed observer is simulated and compared to two alternative observers.

Keywords: Thermoacoustics, Rijke tube, Observers, Nonlinearities, Distributed parameter systems.

1. INTRODUCTION

Thermoacoustic instabilities can be a severe issue in combustion chambers, and have been observed in rocket engines, gas turbines, industrial furnaces and afterburners (Correa (1998); Crocco (1969); Macquisten (1995)). They occur due to a positive feedback loop between the heat release from the combustion process and the acoustics in the chamber when these are sufficiently in phase (Putnam and Dennis (1954)). Oscillations can grow into a limit cycle with amplitude large enough to damage the combustion system. However, it is difficult in practice to forecast when or if thermoacoustic instabilities occur for a given combustor (Lieuwen and Yang (2005)), and hence much research effort has been devoted to understanding the phenomenon better, and also developing techniques for monitoring and mitigating the instabilities.

One common experimental setup for studying thermoacoustic instabilities, being one of the simplest arrangements capable of exhibiting the phenomenon, is the electrically heated Rijke tube. It has the advantage of being simple to model due to the absence of complicated combustion dynamics. The Rijke tube (with a flame) was first introduced in Rijke (1859), and has since been the subject of numerous studies to gain understanding of and develop methods to mitigate thermoacoustic instabilies, see Raun et al. (1993) for a review.

Much of the previous work on the Rijke tube has consisted in characterizing its stability limits, with Carrier (1955) pioneering linear stability analysis of the system and later Bayly (1986) taking into account nonlinear features. In addition to experimental studies of the stability limits of the Rijke tube, studies on active control strategies applied to attenuate the thermoacoustic oscillations in the Rijke tube have been performed. A control law consisting of measuring the pressure signal upstream of the heater and subsequently sending this signal phase-shifted and amplified to a loudspeaker downstreams has been applied to a Rijke tube in Heckl (1988), being one of the first studies investigating active control of the Rijke tube. More recently, a more sophisticated full-state feedback boundary control law designed via infinite-dimensional backstepping on a linearized PDE-ODE model of the electrically heated Rijke tube has been derived in de Andrade et al. (2018b). To pair with this full-state feedback control law, a corresponding boundary observer for the linearized PDE-ODE model is derived in de Andrade et al. (2018a).

A heat release model which, together with an acoustic model, captures the most important behaviour of the electrically heated Rijke tube is King's law (King (1914)). For the observer design in de Andrade et al. (2018a), King's law is linearized, which makes the mathematical analysis tractable - however this linear ODE model does not reflect the full nonlinear dynamics one typically obtains in practice. A nonlinear heat release model is needed to model the saturated response one sees for large amplitudes and resultant limit cycle behaviour (Agostino et al. (2002)). To maintain this behaviour in the design, we propose a differ-

⋆ The work of N.C.A. Wilhelmsen has received funding through the European Union's Horizon 2020 research and innovation programme under the Marie Skłodowska-Curie grant agreement No. 766264.

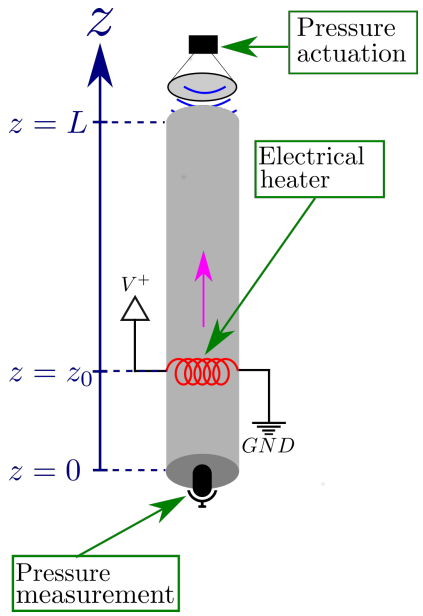

Fig. 1. Electrically heated vertical Rijke tube. The magenta arrow represents base flow induced by the electrical heater.

ent observer taking into account the nonlinear features of King's law. This is the main contribution of the paper.

Our approach is as follows. We design an observer by injecting measured signals at two boundaries of an infinite dimensional observer. The zero equilibrium of the resulting error system is shown to be Globally Asymptotically Stable (GAS). Further, we show that the presence of uncertainty in the boundary acoustic impedance results in bounded errors.

The paper is organized in the following way. In Section 2 the governing equations are introduced and the problem we are solving is defined. Next, in Section 3 the design and convergence analysis of the observer is covered. Results from simulations are presented in Section 4 before some concluding remarks are offered in Section 5.

2. PROBLEM STATEMENT

Consider a vertical Rijke tube of length L and constant circular cross-sectional area A with an electrical heater placed at a fixed vertical position $z_0 \in (0, \frac{L}{2})$ [1]. The phenomenon we are studying evolves mainly in the vertical direction inside the Rijke tube, so we use one-dimensional (1D) first principles to model the dynamics of the air column inside the tube (de Andrade et al. (2018b)). To establish an acoustic model, define pressure perturbation $\breve{P} := P - \bar{P}$, velocity perturbation $\breve{V} := V - \bar{V}$, and heat fluctuation $\breve{Q} := Q - \bar{Q}$, with P total pressure, $\bar{P}$ constant atmospheric pressure, V total velocity, $\bar{V}$ constant base flow velocity, Q heat release and $\bar{Q}$ its constant mean value. Also, the mean air density is denoted $\bar{\rho}$. We write, as in Epperlein et al. (2015), the linearized mass, momentum and energy conservation laws of 1D gas dynamics to obtain the following linear acoustic model,

$$\partial_t \breve{V}(z,t) + \frac{1}{\bar{\rho}}\partial_z \breve{P}(z,t) = 0 \tag{1a}$$

$$\partial_t \breve{P}(z,t) + \gamma \bar{P}\partial_z \breve{V}(z,t) = \frac{\bar{\gamma}}{A}\delta(z-z_0)\breve{Q}(t) \tag{1b}$$

$$\breve{P}(L,t) = Z\breve{V}(L,t) + U(t) \tag{1c}$$

$$\breve{P}(0,t) = -Z\breve{V}(0,t) \tag{1d}$$

$$\breve{P}(x,0) = \breve{P}_0(x) \tag{1e}$$

$$\breve{V}(x,0) = \breve{V}_0(x), \tag{1f}$$

defined over the spatial domain $z \in [0, L]$ and for time $t \geq 0$, initialized from $\breve{P}_0, \breve{V}_0 \in L_2(0, L)$. Also, γ is the adiabatic constant, $\bar{\gamma} := \gamma - 1$, Z is an acoustic impedance at the tube boundaries and U is a boundary gauge pressure actuation signal.

To describe the heat release rate Q from the electrical heater, King's law (King (1914)) is used, which together with dynamics described in Lighthill (1954) reads

$$\dot{Q}(t) = -\frac{1}{\tau}Q(t) + \frac{1}{\tau}l_w(\kappa + \kappa_v\sqrt{|V(z_0,t)|})(T_w - T_g) \tag{2a}$$

$$Q(0) = Q_0, \tag{2b}$$

and is initialized from $Q_0 \in \mathbb{R}$, with τ a time-constant due to the boundary layer formed around the electrical heater, l_w the length of the heating wire, T_w is the wire temperature, T_g is the time-averaged gas temperature around z_0, κ is the thermal conductivity of air and κ_v is an empirically determined constant. The model (2) captures the two most important dynamic features required of the heat source for thermoacoustic instabilities to occur, namely a time lag between changes in the local velocity and the heat release rate, and also a positive dependency between the time derivative of the heat release rate and the local air speed. Unlike previous attempts at designing observers for the Rijke tube, as in de Andrade et al. (2018a), we do not linearize King's law in (2) to capture the full nonlinearity of its dynamics.

Hence, given the Rijke tube thermoacoustic model (1)–(2), the objective of this paper is to design an observer producing convergent state estimates $\hat{P}$, $\hat{V}$ and $\hat{Q}$ of respectively the pressure P, velocity V and heat release Q, assuming the boundary pressure measurement

$$Y(t) := \breve{P}(0,t) \tag{3}$$

is available, only. As noted in Epperlein et al. (2015), in practice the nodes in the Rijke tube are situated slightly outside the tube ends. Hence by placing the pressure sensor right by the tube opening or slightly inside, the node is avoided and one obtains information that can be used for state estimation. Next, we proceed with the observer design and assess its convergence properties.

3. OBSERVER DESIGN

3.1 Model in Riemann coordinates

For the observer design and analysis, we rewrite the linearized acoustics (1) in Riemann invariant coordinates and fold the spatial domain around z_0 to move the heat release to the system boundary. To facilitate this, we introduce the invertible linear spatial coordinate transforms $z_i : x \mapsto z$,

[1] A necessary condition for thermoacoustic instabilities to occur is for the heater to be in the lower half of the tube.

$$z_1(x) := z_0(1-x) \tag{4a}$$
$$z_2(x) := z_0 + x(L - z_0), \tag{4b}$$

with $x \in [0,1]$ and $i \in \{1,2\}$. The subscript i denotes which part of the Rijke tube x is mapped to, with z_1 mapping x to points below the electrical heater and z_2 mapping x to points above the electrical heater. Next, define the Riemann coordinates

$$u_i(x,t) := \breve{P}(z_i(x),t) + k\breve{V}(z_i(x),t) \tag{5a}$$
$$v_i(x,t) := \breve{P}(z_i(x),t) - k\breve{V}(z_i(x),t). \tag{5b}$$

where

$$k := \sqrt{\gamma \bar{P}\bar{\rho}}. \tag{6}$$

This allows us to rewrite the linearized acoustics (1a)–(1b) over $(x,t) \in (0,1)\times[0,\infty)$ as

$$\partial_t u_1(x,t) = \lambda_1 \partial_x u_1(x,t), \quad \partial_t u_2(x,t) = -\lambda_2 \partial_x u_2(x,t), \tag{7a}$$
$$\partial_t v_1(x,t) = -\lambda_1 \partial_x v_1(x,t), \quad \partial_t v_2(x,t) = \lambda_2 \partial_x v_2(x,t), \tag{7b}$$

where

$$\lambda_1 := \frac{\lambda}{z_0}, \qquad \lambda_2 := \frac{\lambda}{L - z_0}, \qquad \lambda := \sqrt{\frac{\gamma \bar{P}}{\bar{\rho}}}, \tag{8}$$

with λ being the speed of sound inside the tube.

Remark 1. Since $z_0 \leq \frac{L}{2}$, we have that $\lambda_1 \geq \lambda_2$. This fact is useful later on in the observer design.

Next, the acoustics boundary conditions (1c)–(1d) are rewritten as

$$u_2(0,t) = u_1(0,t) + \mu\breve{X}(t), \quad v_1(0,t) = v_2(0,t) + \mu\breve{X}(t), \tag{9a}$$
$$u_1(1,t) = dv_1(1,t), \qquad v_2(1,t) = du_2(1,t) + W(t), \tag{9b}$$

where we have denoted $\breve{X} := \breve{Q}$, the boundary reflection coefficient d, the ODE boundary coefficient μ and input signal W, are respectively defined

$$d := \frac{Z-k}{Z+k}, \quad \mu := \frac{k\bar{\gamma}}{\gamma A \bar{P}}, \quad W(t) := (1-d)U(t). \tag{10}$$

Denoting $X := Q$, the heat release model (2) is also rewritten as

$$\dot{X}(t) = -aX(t) + b_1\sqrt{|b_2 + b_3[u_1(0,t) - v_2(0,t)]|} + b_4 \tag{11}$$

with

$$a := \frac{1}{\tau}, \qquad b_1 := \frac{l_w(T_w - T_g)\kappa_v}{\tau}, \qquad b_2 := \bar{V}, \tag{12a}$$
$$b_3 := \frac{1}{2k}, \qquad b_4 := \frac{l_w(T_w - T_g)\kappa}{\tau}. \tag{12b}$$

The gauge pressure measurement (3) can in the Riemann invariant coordinates (5) be written as $Y(\cdot) = \frac{1}{2}(u_1(1,\cdot) + v_1(1,\cdot))$. Applying the boundary condition for u_1 we see by defining the boundary measurement signal

$$y(t) := v_1(1,t) \tag{13}$$

the gauge pressure measurement can be reconstructed as $Y = \frac{1+d}{2}y$. These dynamics are schematically depicted in Figure 2. Notice that several feedback loops make the dynamics potentially unstable.

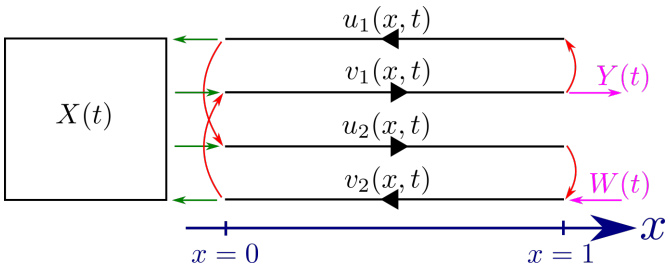

Fig. 2. Schematic of Rijke tube system in Riemann coordinates. The green arrows are couplings between the ODE state and PDE states, the red arrows are boundary couplings between the PDE states and the magenta arrows represent input and output signals.

3.2 Proposed observer

With the measurement signal y defined in (13), we propose the following observer

$$\dot{\hat{X}}(t) = -a\hat{X}(t) + b_1\sqrt{|b_2 + b_3[\hat{u}_1(0,t) - \hat{v}_2(0,t)]|} + b_4 \tag{14a}$$
$$\partial_t \hat{u}_1(x,t) = \lambda_1 \partial_x \hat{u}_1(x,t) \tag{14b}$$
$$\partial_t \hat{u}_2(x,t) = -\lambda_2 \partial_x \hat{u}_2(x,t) \tag{14c}$$
$$\partial_t \hat{v}_1(x,t) = -\lambda_1 \partial_x \hat{v}_1(x,t) \tag{14d}$$
$$\partial_t \hat{v}_2(x,t) = \lambda_2 \partial_x \hat{v}_2(x,t) \tag{14e}$$
$$\hat{u}_2(0,t) = \hat{u}_1(0,t) + \mu(\hat{X}(t) - \bar{X}) \tag{14f}$$
$$\hat{v}_1(0,t) = \hat{v}_2(0,t) + \mu(\hat{X}(t) - \bar{X}) \tag{14g}$$
$$\hat{u}_1(1,t) = dy(t) \tag{14h}$$
$$\hat{v}_2(1,t) = dy(t + \lambda_1^{-1} - \lambda_2^{-1}) + W(t) + d\left(\hat{u}_1(0,t-\lambda_2^{-1}) - \hat{v}_2(0,t-\lambda_2^{-1})\right). \tag{14i}$$

We state now the main result of this paper, which pertains to the convergence properties of (14), before explaining the rationale behind the observer followed by a formal proof of the result.

Theorem 3.1. Consider system (7)–(12), and the state observer (14) using the measurement (13). Assume they have initial conditions $(u_{i,0}, v_{i,0}, X_0) \in L^2(0,1)\times L^2(0,1)\times\mathbb{R}$ and $(\hat{u}_{i,0}, \hat{v}_{i,0}, \hat{X}_0) \in L^2(0,1)\times L^2(0,1)\times\mathbb{R}$, respectively. Then, the zero equilibrium of the dynamics of the estimation errors $\tilde{u}_i := u_i - \hat{u}_i$, $\tilde{v}_i := v_i - \hat{v}_i$, $\tilde{X} := X - \hat{X}$ is GAS.

This observer consists of a copy of the Rijke tube dynamics in Riemann coordinates (7)–(12), with the exception of (14h)–(14i). While (14h) consists of injecting the measured output directly, Equation (14i) deserves more explanation. It is based on the following considerations. First, notice that substituting Equation (9a) into the general solution of u_2 in terms of the boundary at $x = 0$, $u_2(1,t)$ rewrites

$$u_2(1,t) = u_2(0, t-\lambda_2^{-1}) = u_1(0,t-\lambda_2^{-1}) + \mu\breve{X}(t-\lambda_2^{-1}) \tag{15}$$

Besides, using the expression for $v_1(0,t)$ from (9a) together with the measurement $y(t) = v_1(1,t)$ yields

$$\mu\breve{X}(t) = y(t + \lambda_1^{-1}) - v_2(0,t) \tag{16}$$

Combining (9b), (15) and (16) yields

$$v_2(1,t) = d\left[u_1(0,t-\lambda_2^{-1}) - v_2(0,t-\lambda_2^{-1})\right.$$

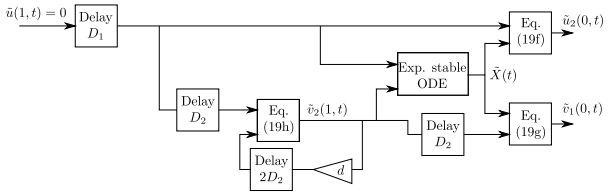

Fig. 3. Schematic of the error system signals. The only internal feedback is $\tilde{v}_2(1,\cdot)$ feeding into itself.

$$+y(t+\lambda_1^{-1}-\lambda_2^{-1})\big] + W(t) \tag{17}$$

The boundary condition (14i) follows by considering estimates of $u_1(0,t-\lambda_2^{-1})$ and $v_2(0,t-\lambda_2^{-1})$ in lieu of the true values. As we show in the next Section, the resulting error converges asymptotically to zero.

Remark 2. Notice that the observer is causal, in particular the signal $y(t+\lambda_1^{-1}-\lambda_2^{-1})$ is available at time t due to Remark 1.

3.3 Convergence analysis

The most critical boundary conditions in the error system for stability are $\tilde{u}_1(1,\cdot)$, $\tilde{v}_2(1,\cdot)$, so we derive their expressions first. It is trivial to see that $\tilde{u}_1(1,\cdot)=0$, while subtracting (14i) from (17) yields

$$\tilde{v}_2(1,t) = d\left(\tilde{u}_1(0,t-\lambda_2^{-1}) - \tilde{v}_2(0,t-\lambda_2^{-1})\right). \tag{18}$$

The other terms in the observer (14) are copies of the corresponding terms in the original system (7)–(12) and hence their corresponding error dynamics are easily computed. Therefore, the state estimation error in $\tilde{u}_i, \tilde{v}_i, \tilde{X}$ satisfies the dynamics

$$\partial_t \tilde{u}_1(x,t) = \lambda_1 \partial_x \tilde{u}_1(x,t) \tag{19a}$$
$$\partial_t \tilde{u}_2(x,t) = -\lambda_2 \partial_x \tilde{u}_2(x,t) \tag{19b}$$
$$\partial_t \tilde{v}_1(x,t) = -\lambda_1 \partial_x \tilde{v}_1(x,t) \tag{19c}$$
$$\partial_t \tilde{v}_2(x,t) = \lambda_2 \partial_x \tilde{v}_2(x,t) \tag{19d}$$
$$\tilde{u}_1(1,t) = 0 \tag{19e}$$
$$\tilde{u}_2(0,t) = \tilde{u}_1(0,t) + \mu\tilde{X}(t) \tag{19f}$$
$$\tilde{v}_1(0,t) = \tilde{v}_2(0,t) + \mu\tilde{X}(t) \tag{19g}$$
$$\tilde{v}_2(1,t) = d\left(\tilde{u}_1(0,t-\lambda_2^{-1}) - \tilde{v}_2(0,t-\lambda_2^{-1})\right) \tag{19h}$$
$$\dot{\tilde{X}}(t) = -a\tilde{X}(t) + b_1\sqrt{|b_2 + b_3[u_1(0,t) - v_2(0,t)]|} - b_1\sqrt{|b_2 + b_3[\hat{u}_1(0,t) - \hat{v}_2(0,t)]|}. \tag{19i}$$

A schematic view of the error system is shown in Figure 3, illustrating the cascade structure of its dynamics which ensure the convergence of its states to zero. We are now ready to prove Theorem 3.1.

Proof. [Proof of Theorem 3.1] From (19a), (19e) we see that $\tilde{u}_1(0,t-\lambda_2^{-1})=0$ for time $t \geq \lambda_1^{-1}+\lambda_2^{-1}$. Hence the boundary condition (19h) simplifies after this time to

$$\tilde{v}_2(1,t) = -d\tilde{v}_2(0,t-\lambda_2^{-1}) \tag{20}$$

allowing us to conclude that

$$\tilde{v}_2(0,t) = -d\tilde{v}_2(0,t-2\lambda_2^{-1}). \tag{21}$$

Since $|d|<1$, we can conclude that $\tilde{v}_2(0)\to 0$ exponentially as $t\to\infty$. Next, we can bound (19i) by the following inequality:

$$\dot{\tilde{X}}(t) \leq -a\tilde{X}(t) + b_1\sqrt{|b_3[\tilde{u}_1(0,t) - \tilde{v}_2(0,t)]|}. \tag{22}$$

Define

$$g(t) := b_1\sqrt{|b_3\iota(t)|}, \qquad \iota(t) := \tilde{u}_1(0,t) - \tilde{v}_2(0,t) \tag{23}$$

where we know g tends to zero as $t\to\infty$. Also, defining the linear system in $\tilde{\Xi}$,

$$\dot{\tilde{\Xi}}(t) = -a\tilde{\Xi}(t) + g(t), \tag{24}$$

with initial condition $\tilde{\Xi}(0) = \tilde{X}(0)$, then $\tilde{\Xi}$ is Input-to-State Stable (ISS) with respect to g. More precisely (see Khalil and Grizzle (2002)), we can establish the bound (where $0\leq t_0\leq t$),

$$|\tilde{\Xi}(t-t_0)| \leq e^{-a(t-t_0)}|\tilde{\Xi}(t_0)| + \frac{1}{a}\sup_{t_0\leq\tau\leq t}|g(\tau)|. \tag{25}$$

Since $\dot{\tilde{X}} \leq \dot{\tilde{\Xi}}$ and $\tilde{X}(0)=\tilde{\Xi}(0)$, we can establish

$$\tilde{X}(t) \leq \tilde{\Xi}(t). \tag{26}$$

As g is exponentially vanishing as $t\to\infty$, we see the right hand side of (25) goes to zero and hence $\tilde{X}\to 0$ asymptotically as $t\to\infty$, which proves the Theorem.

3.4 Robustness to modelling error in boundary condition

In practice the acoustic impedance Z appearing in Equations (1c)–(1d) is difficult to estimate correctly, implying the boundary coefficient d appearing in (9b) for the Riemann coordinate formulation is prone to being incorrectly modelled. Denote the estimate of d as $\hat{d}$, and define $\tilde{d} := d - \hat{d}$ as the modelling error.

When $\hat{d}$ is used in place of d in the observer (14), the expressions for $\tilde{u}_1(1)$, $\tilde{v}_2(1)$, given by (19e), (19h), change to

$$\tilde{u}_1(1,t) = \tilde{d}y(t) \tag{27}$$
$$\tilde{v}_2(1,t) = \hat{d}(\tilde{u}_1(0,t-\lambda_2^{-1}) - \tilde{v}_2(0,t-\lambda_2^{-1}) + \tilde{d}\left(\mu X(t-\lambda_2^{-1}) + u_1(0,t-\lambda_2^{-1})\right) \tag{28}$$

with the rest of the error system (19) being unaffected. We state now a Proposition on the sensitivity of the state estimate error to errors in modelling this boundary condition.

Proposition 3.2. Assume that the states of the original system are bounded, and the estimate $\hat{d}$ of d satisfies

$$|\hat{d}| < 1. \tag{29}$$

Then all the error signals $\tilde{u}_i$, $\tilde{v}_i$, $\tilde{X}$ are bounded.

Proof. In the following we denote the Laplace transform of the time-domain signal f as $\check{f}$, i.e. $\check{f}(s) = \mathcal{L}(f(\cdot))$. With the signal h defined as

$$h(t) := u_1(0,t) + \mu X(t) \tag{30}$$

we find that

$$\begin{bmatrix}\check{\tilde{u}}_1(0,s)\\ \check{\tilde{v}}_2(0,s)\end{bmatrix} = H(s)\begin{bmatrix}\check{y}(s)\\ \check{h}(s)\end{bmatrix} \tag{31}$$

where

$$H(s) := \begin{bmatrix}\tilde{d}e^{-\lambda_1^{-1}s} & 0\\ \frac{\hat{d}e^{-(2\lambda_2^{-1}+\lambda_1^{-1})s}}{1+\hat{d}e^{-2\lambda_2^{-1}s}} & \frac{e^{-2\lambda_2^{-1}s}}{1+\hat{d}e^{-2\lambda_2^{-1}s}}\end{bmatrix} \tag{32}$$

is a transfer matrix. This allows us to reconstruct the signal ι defined in (23) in terms of signals y, h as

$$\iota(t) = \begin{bmatrix}1\\ -1\end{bmatrix}^T \mathcal{L}^{-1}\left(H(s)\begin{bmatrix}\check{y}(s)\\ \check{h}(s)\end{bmatrix}\right) \tag{33}$$

Since $|\hat{d}| < 1$, Equation (32) implies that H is stable (see Niculescu (2001) for a more extended treatment of transfer functions for systems with time delays), and since $y, h \in L^\infty$, one has $\iota, g \in L^\infty$, with g defined by (23).

Further, since $\tilde{u}_1(1,\cdot) = \tilde{d}y(\cdot)$, $\tilde{u}_1(1,\cdot) \in L^\infty$ and hence all of $\tilde{u}_1$ is bounded. Besides, one has

$$\check{\tilde{v}}_2(1,s) = \frac{\tilde{d}e^{-\lambda_2^{-1}s}}{1+\hat{d}e^{-\lambda_2^{-1}s}}\left(\hat{d}\check{y}(s)e^{-\lambda_1^{-1}s} + \check{h}(s)\right) \tag{34}$$

which again using that $|\hat{d}| < 1$ implies that $\tilde{v}_2(1,\cdot) \in L^\infty$ and therefore all of $\tilde{v}_2$ is bounded. Equation (22) further implies the following bound on $\tilde{X}$,

$$\tilde{X}(t) \leq e^{-at}|\tilde{X}(0)| + \frac{1}{a}||g||_\infty. \tag{35}$$

Finally, (19f)–(19g) express $\tilde{u}_2(0,\cdot)$, $\tilde{v}_1(0,\cdot)$ as the sum of bounded signals, therefore $\tilde{u}_2(x,\cdot), \tilde{v}_1(x,\cdot) \in L^\infty$, $\forall x \in [0,1]$.

4. SIMULATIONS

In this section the observer (14) is tested in simulations implemented in `MATLAB`. The proposed observer has certain advantages, such as being guaranteed stable for all system parameters, global asymptotic convergence and being robust to modelling errors in the boundary condition d. However, it also has certain drawbacks, such as having no tuning parameters to calibrate and possible poor measurement noise filtering properties as the measurement is injected directly.

For comparison we test, where possible, the observer from this paper with two alternative observers:

(1) A "trivial" observer identical to the observer (14), except the boundary condition $\hat{v}_2(1,\cdot) = d\hat{u}_2(1,\cdot) + W(\cdot)$ is used in place of (14i).
(2) A nonlinear observer consisting of the "trivial" observer together with observer gains from de Andrade et al. (2018a), multiplied by the output estimation error $(y(\cdot) - \hat{v}_1(1,\cdot))$ and added to the observer dynamics (14a)–(14e).

A total of three different simulations scenarios are presented. In the first two simulations, the Rijke tube model (1)–(2) is implemented with parameters that incite thermaocoustic instabilities. No actuation signal is imposed on the top boundary so we assume $U = 0$. The physical parameters used are summarized in Table 1. For the observers in the first simulation, it is assumed all system parameters are known exactly, but in the second simulation an incorrect value of Z is used in the observers. Lastly, results from a toy simulation, that implements the system (7), (9), (11), together with the observer (14) and observers mentioned above, is presented. This demonstrates that observer (14) in this paper works for certain system parameters the alternative observers do not work for, due to them having no proven stability guarantee.

All results presented are from simulations that integrate the equations for a total of 1 second, with the observers being turned on at time $t = 0.25$ seconds. The PDEs are integrated using a first-order finite difference upwind scheme, while the ODE is integrated with a fourth-order Runge-Kutta scheme. The spatial discretization used is

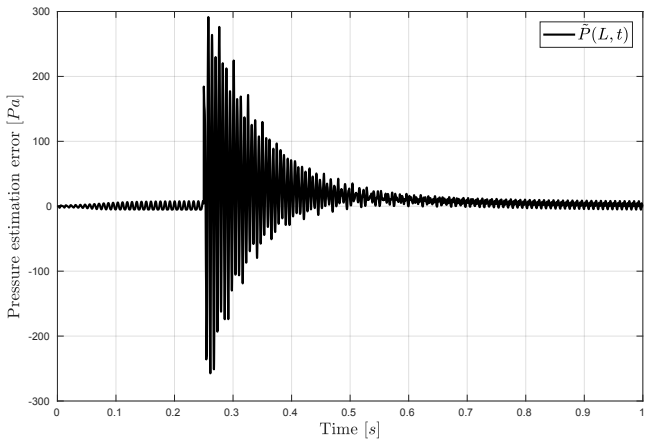

Fig. 4a. Pressure estimation error $\tilde{P}(L,\cdot)$ at tube end opposite from where sensing takes place, for observer (14).

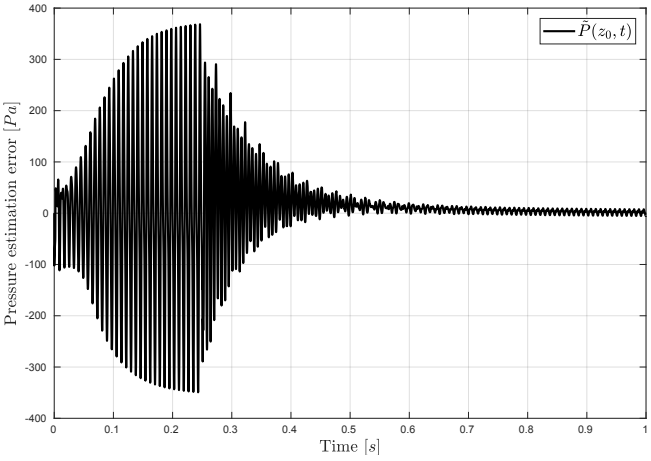

Fig. 4b. Pressure estimation error $\tilde{P}(z_0,\cdot)$ at heater location for observer (14).

$dx = 1.00 \times 10^{-2}$ m, while the temporal discretization is $dt = 8.25 \times 10^{-8}$ s. All observers are initialized to

$$\hat{u}_{1,0}(x) = \sin(2x) \qquad \hat{u}_{2,0}(x) = \cos(3x)$$
$$\hat{v}_{1,0}(x) = e^x \qquad \hat{v}_{2,0}(x) = \sin(5x) - 2\cos(x)$$
$$\hat{X}_0 = 500.$$

4.1 Thermoacoustic simulations with no modelling error

In this simulation it is assumed the observers have perfect knowledge of the system parameters in Table 1. First, to showcase the performance of the proposed observer (14), in Figures 4–6 we see respectively the estimation errors for the pressure $\tilde{P} := P - \hat{P}$ and velocity $\tilde{V} := V - \hat{V}$, evaluated at positions $z = L$, $z = z_0$, and the heat release $\tilde{Q} := Q - \hat{Q}$, all associated with the estimates $\hat{P}$, $\hat{V}$, and $\hat{Q}$ produced by this observer. As predicted by Theorem 3.1, these approach the origin asymptotically as $t \to \infty$.

Next, the transient performance of the various observers in estimating the heat release rate Q is compared. Even though the equations were integrated up to time $t = 1$ second, for clarity a time-interval of length 0.2 seconds around the time the observers are turned on is shown. In

Parameter	Description	Value	Unit
Z	Tube impedence	6	$N\ s\ m^{-3}$
L	Tube length	1.4	m
A	Tube cross-sectional area	0.004	m^2
z_0	Position of heater	0.35	m
l_w	Length of heating wire	1.067	m
T_w	Temperature of wire	933	K
T_g	Temperature of air	300	K
τ	Heating element time constant	2×10^{-3}	s
κ	Thermal conductivity of air	26.38×10^{-3}	$W\ m^{-1}\ K^{-1}$
κ_v	Empirical constant in King's law	1.5	$W\ s^{\frac{1}{2}}\ m^{-\frac{3}{2}}\ K^{-1}$
$\bar{\rho}$	Average air density	1.2	$kg\ m^{-3}$
$\bar{P}$	Atmospheric pressure	10^5	$N\ m^{-2}$
$\bar{V}$	Base flow velocity	0.35	$m\ s^{-1}$
γ	Adiabatic constant	1.4	–

Table 1. Physical parameters used in simulation

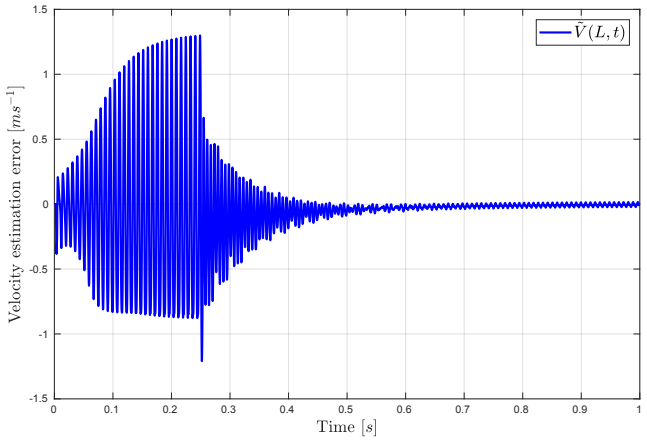

Fig. 5a. Velocity estimation error $\tilde{V}(L,\cdot)$ at tube end opposite from where sensing takes place, for observer (14).

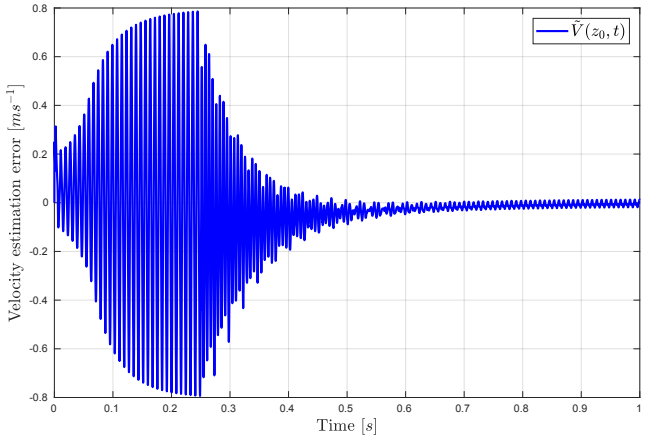

Fig. 5b. Velocity estimation error $\tilde{V}(z_0,\cdot)$ at heater location for observer (14).

Figure 7 the heat release rate estimation error associated with the different observers is displayed for times between $t = 0.24$ and $t = 0.44$ seconds. This interval contains the time instant when the observers are turned on, so the initial behaviour can be seen from this plot. The "trivial" observer seems to converge fastest, with the observer using backstepping gains converging second fastest and the

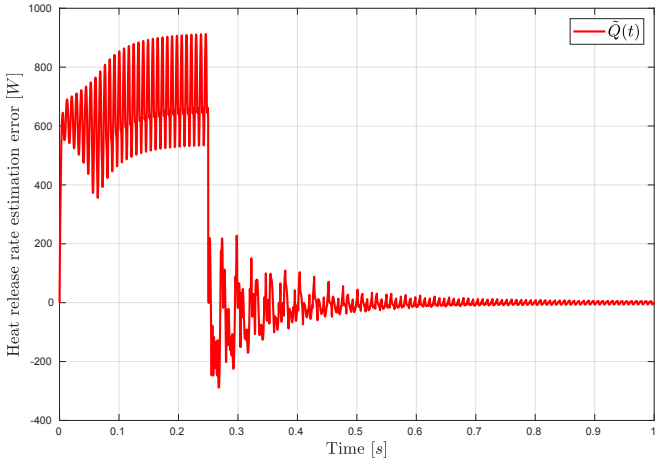

Fig. 6. Heat release rate estimation error $\tilde{Q}$ for observer (14).

observer (14) from this paper converging more slowly, but asymptotically, as is shown in Figure 6.

Interestingly, in this example the observer (14) had overall the worst performance. This can be attributed to the fact that the error $-d\tilde{v}_2(0, t - \lambda_2^{-1})$ is introduced in the boundary for $\hat{v}_2(1)$ to ensure stability, with the trade-off being that the performance is degraded initially, before improving as time increases. Next, the performance of the observers when there is a modelling error in the boundary coefficient is compared.

Remark 3. In this example, the convergence properties of the "trivial" observer and the nonlinear observer using the backstepping gains is similar, showing that the observer gains have little extra effect on the convergence properties.

4.2 Thermoacoustic simulations with modelling error in boundary

Here the observers are tested against modelling error in the reflection coefficient d. Therefore, for this simulation it is assumed the observers have correct knowledge of all the physical parameters in Table 1 except for Z. Instead the observers use an estimate $\hat{Z} = 50$, which gives an estimate $\hat{d} \approx -0.78$.

Overall, the effect of the incorrect knowledge of Z is that the observers have an offset in the state estimate.

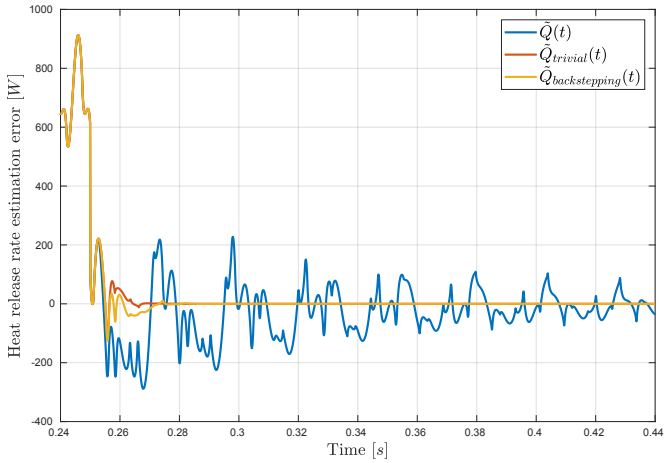

Fig. 7. Heat release rate estimation error $\tilde{Q}$ produced by observer (14), $\tilde{Q}_{trivial}$ produced by the "trivial" observer and $\tilde{Q}_{backstepping}$ produced by the observer from de Andrade et al. (2018a) but using a nonlinear ODE. The plot shows the curves for times $t \in [0.24, 0.44]$.

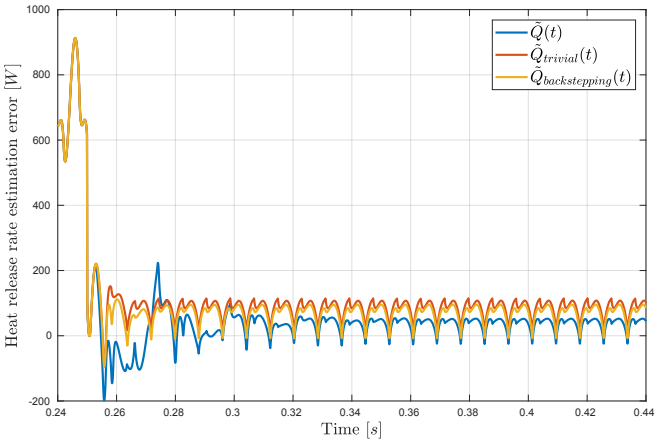

Fig. 8. Heat release rate estimation error $\tilde{Q}$ produced by observer (14), $\tilde{Q}_{trivial}$ produced by the "trivial" observer and $\tilde{Q}_{backstepping}$ produced by the observer from de Andrade et al. (2018a) but using a nonlinear ODE, with all observers having incorrect knowledge of the acoustic boundary Z. The plot shows the curves for times $t \in [0.24, 0.44]$.

The magnitude of this offset for the various observers in estimating the heat release rate can be seen in Figure 8. From this plot it can be seen that the observer (14) has the smallest offset from the correct value, followed by the observer using backstepping gains, and lastly the "trivial" observer has the largest offset. It is interesting to note that despite having incorrect knowledge of the boundary condition, the observer (14) performs better during the transient for the simulation shown here compared to the simulation in Section 4.1. This is due to the smaller magnitude of $\hat{d}$ making the error $-\hat{d}\tilde{v}_2(0, t - \lambda_2^{-1}))$ at the boundary for $\hat{v}_2(1, \cdot)$ shrink faster in the transient.

The simulations suggest the design of the observer (14) makes it more robust to modelling errors in the boundary reflection coefficient d compared to the other two observers. For the observer using backstepping gains, the gains helped make the offset smaller than the offset from the "trivial" observer, but not to the extent that the observer (14) managed. In Proposition 3.2 it was proven that the estimation error produced by the observer (14) when using an incorrect boundary condition would be bounded - for the other two observers this has of yet not been proven.

Another performance aspect that is not necessarily guaranteed for the other two observers is that they converge for all possible system parameters. Next a toy simulation is offered where the observer (14) converges to the correct estimate but the other observers become unstable.

4.3 Toy simulations showing stability for alternative system parameters

Due to the way the boundary condition (14i) is constructed for the observer (14), it is possible to prove that the state estimates produced by this observer converge to their true values. For the trivial observer, due to it having a potentially unstable feedback loop of previous ODE states influencing the dynamics of the current ODE states via the nonlinearity present in King's law, there exists certain parameters for which the observer can become unstable,

Parameter	Value
a	500
b_1	474750000
b_2	3
b_3	0.001
b_4	8349270
d	-0.9711
μ	0.2925
λ_1	975.9
λ_2	325.3

Table 2. Parameters for toy simulation

and the observer in de Andrade et al. (2018a) was only proven to be stable by assuming that the heat release model is linearized.

As a demonstration of what could happen in practice, the system (7), (9), (11) with parameters specified in Table 2 is implemented. Figure 9 shows a plot of the resultant state X, shown in blue, versus the estimate $\hat{X}_{trivial}$ produced by the trivial observer, shown in yellow, and the estimate $\hat{X}$ produced by the observer (14), shown in orange. The estimate produced by the nonlinear observer using backstepping gains from de Andrade et al. (2018a) can not be shown because it becomes unstable very quickly.

As can be seen, the estimate $\hat{X}_{trivial}$ shoots up to values much larger than the range X is oscillating within. The observer (14), however, remains unscathed and produces an estimate $\hat{X}$ that tracks the state X fairly well, asymptotically.

5. CONCLUSIONS

An observer taking into account both the nonlinearity of the heat release model and distributed states of the tube acoustics has been derived for the electrically heated vertical Rijke tube. Instead of applying a standard observer design procedure the observer was designed simply

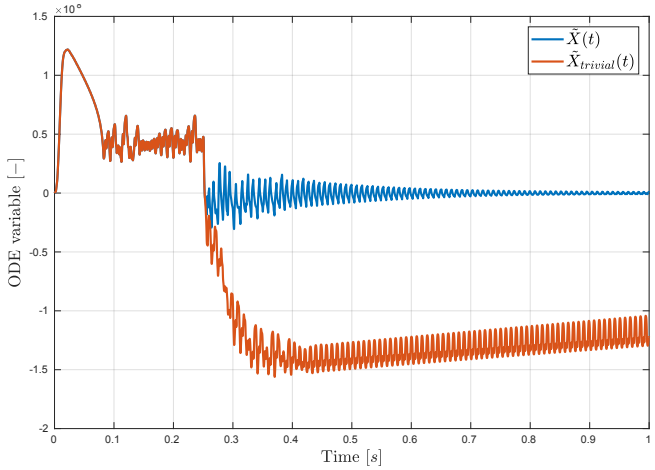

Fig. 9. ODE state estimation error $\tilde{X}$ produced by the observer (14) and $\tilde{X}_{trivial}$ produced by the trivial observer, for a toy example.

by copying the system dynamics and reconstructing some of its boundary conditions from known signals.

It was proven that this observer converges to the origin asymptotically and that it is robust to modelling errors in the boundary condition. Simulations were offered to demonstrate the observer in three examples. Compared to an observer that only injects the measurement at a single boundary, the observer from this paper does not suffer the same problem of blowing up for certain system parameters.

As further work, simulating the observer against a more realistic flow model, such as the nonlinear gas dynamics model based on mass, momentum and energy balance given in Epperlein et al. (2015), would give more insight about the observer performance from a practical standpoint. Also, observer design for the Rijke tube using a flame rather than electrical heater model could be a viable research direction.

ACKNOWLEDGEMENTS

The authors would like to thank Laurent Praly for his insightful comments on the observer design.

REFERENCES

Agostino, F., Baldini, G., Bittanti, S., De Marco, A., Poncia, G., Prandoni, W., and Scarpellini, M. (2002). Nonlinear identification of thermoacoustic instabilities with limit cycles in a rijke tube. In *Proceedings of the International Conference on Control Applications*, volume 2, 1147–1152. IEEE.

Bayly, B.J. (1986). Onset and equilibration of oscillations in general rijke devices. *The Journal of the Acoustical Society of America*, 79(3), 846–851.

Carrier, G. (1955). The mechanics of the rijke tube. *quarterly of Applied Mathematics*, 12(4), 383–395.

Correa, S.M. (1998). Power generation and aeropropulsion gas turbines: From combustion science to combustion technology. In *Symposium (International) on Combustion*, volume 27, 1793–1807. Elsevier.

Crocco, L. (1969). Research on combustion instability in liquid propellant rockets. In *Symposium (International) on Combustion*, volume 12, 85–99. Elsevier.

de Andrade, G.A., Vazquez, R., and Pagano, D.J. (2018a). Backstepping-based linear boundary observer for estimation of thermoacoustic instabilities in a rijke tube. In *2018 IEEE Conference on Decision and Control (CDC)*, 2164–2169. IEEE.

de Andrade, G.A., Vazquez, R., and Pagano, D.J. (2018b). Backstepping stabilization of a linearized ode–pde rijke tube model. *Automatica*, 96, 98–109.

Epperlein, J.P., Bamieh, B., and Astrom, K.J. (2015). Thermoacoustics and the rijke tube: Experiments, identification, and modeling. *IEEE Control Systems*, 35(2), 57–77.

Heckl, M.A. (1988). Active control of the noise from a rijke tube. *Journal of Sound and Vibration*, 124(1), 117–133.

Khalil, H.K. and Grizzle, J.W. (2002). *Nonlinear systems*, volume 3. Prentice hall Upper Saddle River, NJ.

King, L.V. (1914). Xii. on the convection of heat from small cylinders in a stream of fluid: Determination of the convection constants of small platinum wires with applications to hot-wire anemometry. *Phil. Trans. R. Soc. Lond. A*, 214(509-522), 373–432.

Lieuwen, T.C. and Yang, V. (2005). *Combustion instabilities in gas turbine engines: operational experience, fundamental mechanisms, and modeling*. American Institute of Aeronautics and Astronautics.

Lighthill, M.J. (1954). The response of laminar skin friction and heat transfer to fluctuations in the stream velocity. *Proc. R. Soc. Lond. A*, 224(1156), 1–23.

Macquisten, M. (1995). Combustion oscillations in a twin-stream afterburner. *Journal of sound and vibration*, 188(4), 545–560.

Niculescu, S.I. (2001). *Delay effects on stability: a robust control approach*, volume 269. Springer Science & Business Media.

Putnam, A.A. and Dennis, W.R. (1954). Burner oscillations of the gauze-tone type. *The Journal of the Acoustical Society of America*, 26(5), 716–725.

Raun, R., Beckstead, M., Finlinson, J., and Brooks, K. (1993). A review of rijke tubes, rijke burners and related devices. *Progress in Energy and Combustion Science*, 19(4), 313–364.

Rijke, P.L. (1859). Lxxi. notice of a new method of causing a vibration of the air contained in a tube open at both ends. *The London, Edinburgh, and Dublin Philosophical Magazine and Journal of Science*, 17(116), 419–422.